



Study on Simulation of ATLAS ITK Strips

Kunlin Ran, Wuhan University, China

Supervisor: Nicholas Styles, ATLAS Group, DESY

September 7, 2016

Abstract

This report talks about the detector ATLAS construction at the Large Hadron Collider (LHC) at CERN, emphatically introduces the Inner Detector of ATLAS; Then the High Luminosity LHC and ATLAS Upgrade projects are introduced, also the full chain of generating Monte Carlo samples used in ATLAS is summarized. The Study mainly focus on the Strip Detector newly designed in ATLAS Upgrade project. When a particle traverses the detector, the responding cluster number would be shifted by 1 because of silicon strip sensors architecture. This effect on tracking is discussed in the page by doing simulations of shifting strip number by ± 1 with a particular probability (7 %). And optimizations should be decided to mitigate the effects.

Contents

1	ATLAS Introduction	3
1.1	The Inner Detector	4
2	The HL-LHC and ATLAS Upgrade projects	5
2.1	ITK strip	6
2.2	ITK Layout	6
3	Simulation/Digitization/Reconstruction	6
4	Experiment	10
5	Conclusion	16

1 ATLAS Introduction

ATLAS is one of the four major experiments at the Large Hadron Collider (LHC) at CERN. It is a general-purpose particle physics experiment run by an international collaboration and, together with CMS, is designed to exploit the full discovery potential and the huge range of physics opportunities that the LHC provides.[5] See Figure 1.

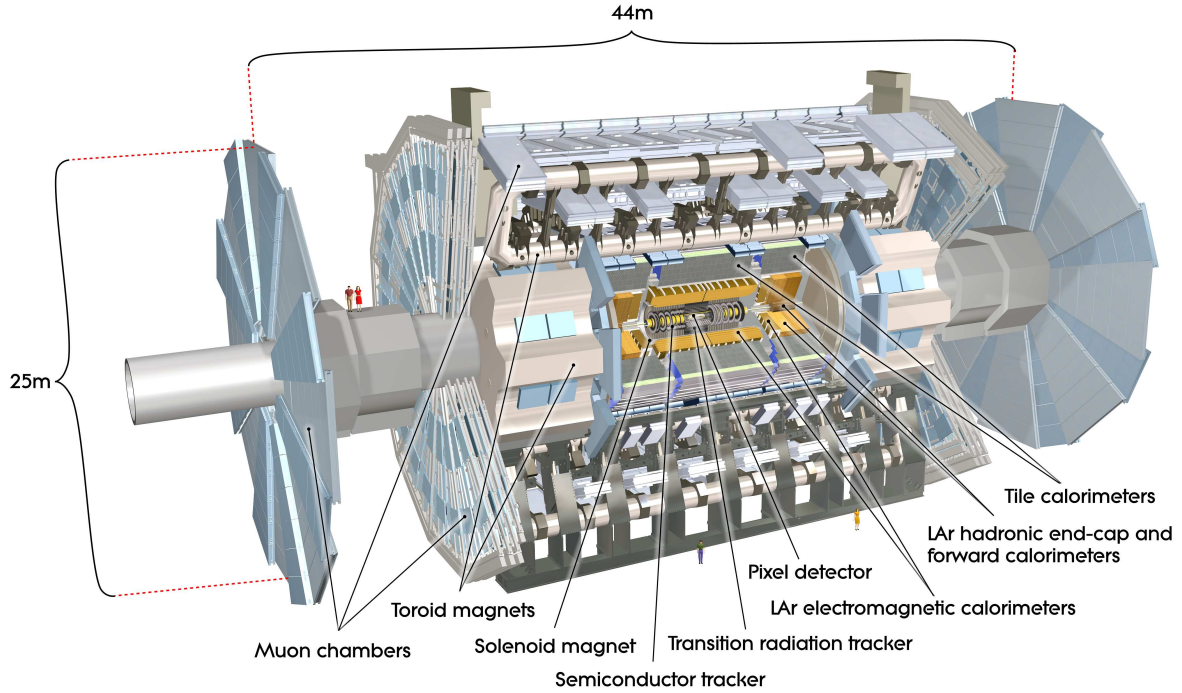


Figure 1: View of the ATLAS detector. The dimensions of the detector are ~ 25 m in height and ~ 44 m in length. The overall weight of the detector is approximately 7000 tonnes.

The largest volume detector ever constructed for a particle collider, ATLAS has the dimensions of a cylinder, 46 m long, 25 m in diameter, and sits in a cavern 100 m below ground. The ATLAS detector weighs 7000 tonnes, similar to the weight of the Eiffel Tower.[6]

The detector itself is a many-layered instrument designed to detect some of the tiniest yet most energetic particles ever created on earth. It consists of six different detecting subsystems wrapped concentrically in layers around the collision point to record the trajectory, momentum, and energy of particles, allowing them to be individually identified and measured. (Inner Detector, Calorimeter, Muon Spectrometer, Magnet System, Trigger and Data Acquisition System and Computing System) A huge magnet system bends the paths of the charged particles so that their momenta can be measured as precisely as possible.

1.1 The Inner Detector

The inner detector is the first part of ATLAS to see the decay products of the collisions, so it is very compact and highly sensitive. It consists of three different systems of sensors all immersed in a magnetic field parallel to the beam axis. The Inner Detector measures the direction, momentum, and charge of electrically-charged particles produced in each proton-proton collision.

The main components of the Inner Detector are: Pixel Detector, Semiconductor Tracker (SCT), and Transition Radiation Tracker (TRT). (See in Figure 1.1).

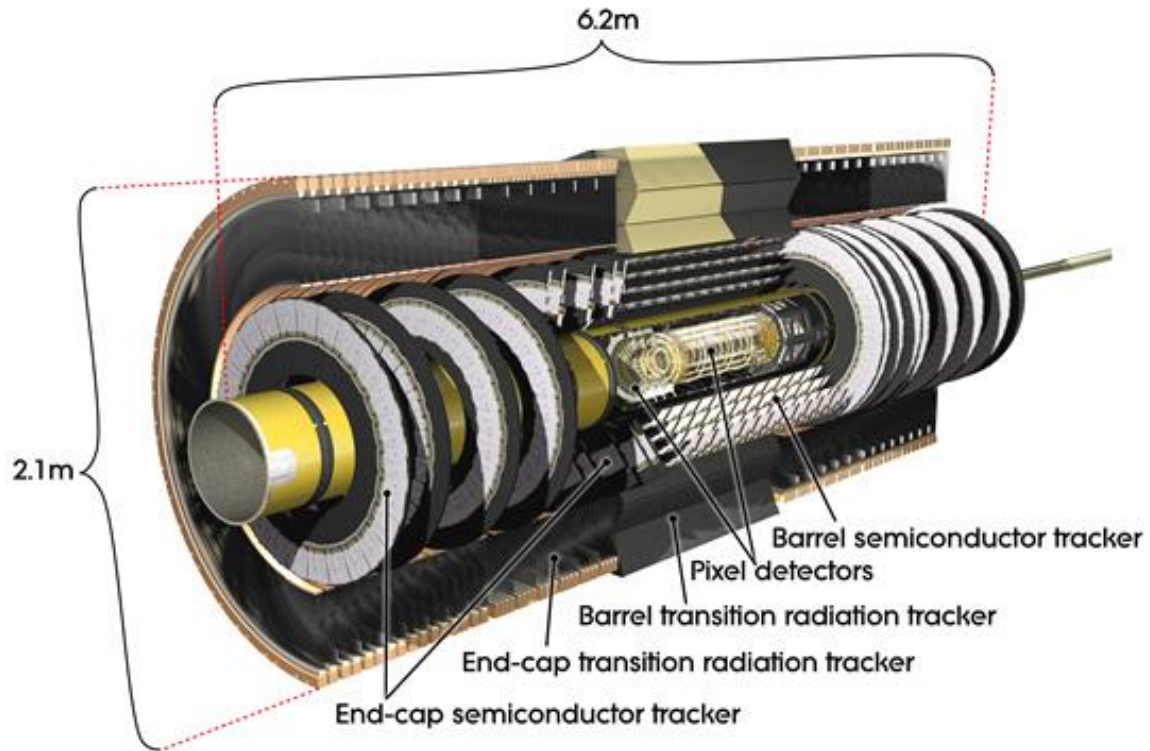


Figure 2: Illustration of ATLAS Inner Detector

Pixel Detector:

- 80 million pixels (80 million channels). Area 1.7 m^2 . 15 kW power consumption;
- Barrel has 1744 modules (10 cm^2) with 46080 readout channels per module;
- Pixel size $50 \times 400 \mu\text{m}^2$. Resolution $14 \times 115 \mu\text{m}^2$
- Three Pixel disks (in each endcap) have 6.6 million channels;
- 3 barrel layers: 1456 modules;
- 3 disks in each end-cap: 288 modules.

Semiconductor Tracker:

- A silicon microstrip tracker consisting of 4088 two-sided modules and over 6 million implanted readout strips (6 million channels);
- 60m² of silicon distributed over 4 cylindrical barrel layers and 18 planar endcap discs;
- Readout strips every 80 μm on the silicon, allowing the positions of charged particles to be recorded to an accuracy of 17 μm per layer (in the direction transverse to the strips)

Transition Radiation Tracker:

- 350000 read-out channels;
- Volume 12m³;
- Basic detector element: straw tube with 4 mm diameter, in the center a 0.03 mm diameter gold-plated tungsten wire;
- 50000 straws in Barrel, each straw 144 cm long. The ends of a straw are read out separately;
- 250000 straws in both endcaps, each straw 39 cm long;
- Precision measurement of 0.17 mm (particle track to wire);
- Provides additional information on the particle type that flew through the detector.

2 The HL-LHC and ATLAS Upgrade projects

ATLAS has been successfully operating in 2010-2012, collecting collision data at $\sqrt{s} = 7$ and 8 TeV, recording an integrated luminosity of $\sim 25\text{fb}^{-1}$ with a peak luminosity of $7.7 \times 10^{33}\text{cm}^{-2}\text{s}^{-1}$. The discovery of a 126 GeV Higgs boson in 2012 is the greatest, even if not the unique, achievement allowing to identify the last piece of the highly successful Standard Model (SM). In the next years, LHC will undergo a series of upgrades leading ultimately to five-fold increase of the instantaneous luminosity with leveling according to the High-Luminosity LHC (HL-LHC) project. The goal is to extend the dataset from about 300 fb^{-1} , expected to be collected by the end of the LHC run (in 2022), to 3000 fb^{-1} by 2035. The foreseen higher luminosity at the HL-LHC is a great challenge for ATLAS. Meeting it will require significant but gradual detector optimizations, changes and improvements, as described here.[4]

The harsher radiation environment and higher detector occupancies at the HL-LHC imply major changes to most of the ATLAS systems, specially those at low radii and large pseudorapidity. A general guideline for these changes is maintaining the same or

improve the detector performance measured at the LHC. The higher event rates and event sizes will be a challenge for the trigger and data acquisition (DAQ) systems, which will require a significant extension of their capacity.

The ATLAS upgrade will be gradual and flexible to accommodate a possible evolution of LHC operational parameters and indications of new physics signals. It is planned in three phases, which correspond to the three long technical shutdowns of the LHC towards the HL-LHC. The Phase-I upgrades are designed to be fully forward-compatible with the physics program of the high luminosity HL-LHC (Phase-II), when the instantaneous luminosity should reach $\sim 5 - 7 \times 10^{34} \text{cm}^{-2}\text{s}^{-1}$, up to 200 interactions per crossing (pile-up) and a total integrated luminosity of 3000 fb^{-1} .

2.1 ITK strip

The current ATLAS Inner Detector (ID) will be re-placed by an all-silicon Inner Tracker (ITk) for the High Luminosity LHC. The strips detector is surrounding the pixels, which is composed of silicon based modules mounted on supporting structures, called staves in the barrel and petals in the end cap discs (see in figure 2.1). The purpose of these structures is to have multi-module support, modularity and integration of cooling and read-out electronics.[2]

Read-out chips are glued on a flex hybrid circuit. The hybrid is then glued on the silicon sensor and wire bonds connect the sensor strips to the chips front-end inputs.

A silicon sensor is made up with 4 segments of 1024 sensor strips each, see in figure 2.1. And every segment has 5 rows of wire bonding pads with $700 \mu\text{m}$ each for read-out. In total, there are 7 % area of the sensor consist of bond pad rows.[3]

2.2 ITK Layout

One of the principle conclusions of the design of layout was that it was indeed possible to build an all-silicon tracker that would be capable of delivering performance that was at least as good as and probably better than the current Inner Detector. The design presented was matched to the physics program that will start at Phase II. Furthermore, it was shown that this is possible in an environment where there are up to 200 proton-proton interactions, per beam crossing, in the middle of the detector.[8]

The following generation of ITk layouts features a complete re-optimization of both the strip and pixel detectors. Take Extended.3.2 for example (see in figure 2.2). There are 5 pixel barrel layers, 4 strip barrel layers and 6 strip endcap disk layers. This layout is optimized for 9 space points up to $|\eta| = 3.2$ as you can see in figure 2.2.

3 Simulation/Digitization/Reconstruction

The production of simulated data is an essential component of experimental particle physics. It allows to probe new theories and test the outcome of those against data taken with the detector. Furthermore it creates the possibility to understand certain

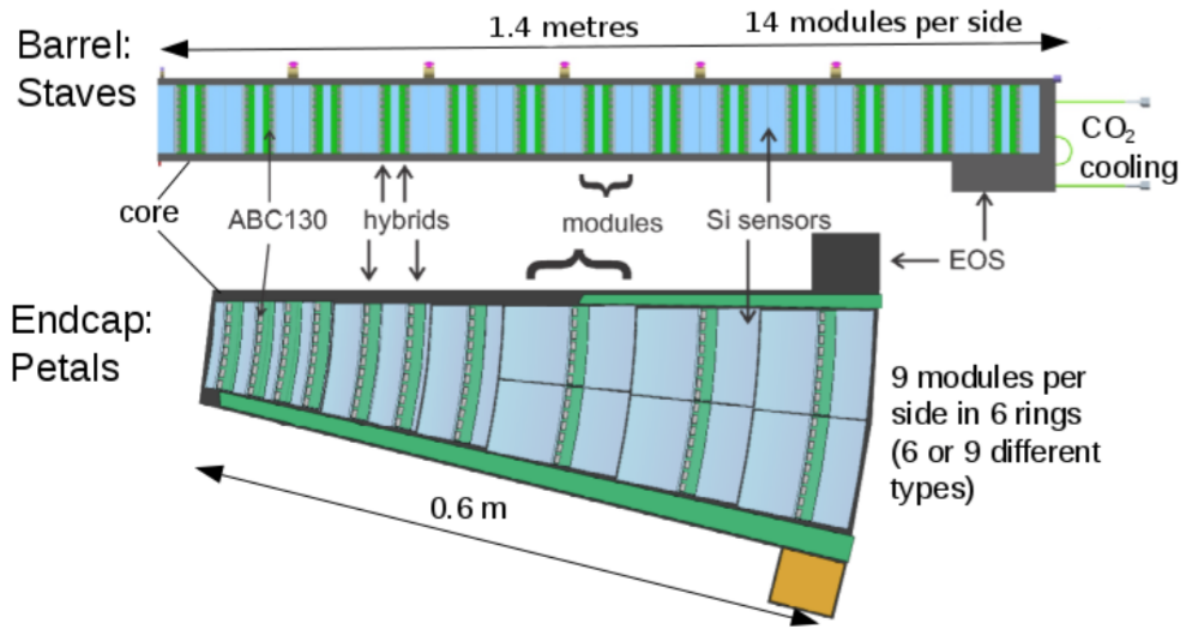


Figure 3: A stave in the barrel and a petal in the end-cap discs, modules are mounted on the structures. The hybrid circuit is glued on silicon sensors and wire-bonds connect the sensor strips to the chips front-end inputs

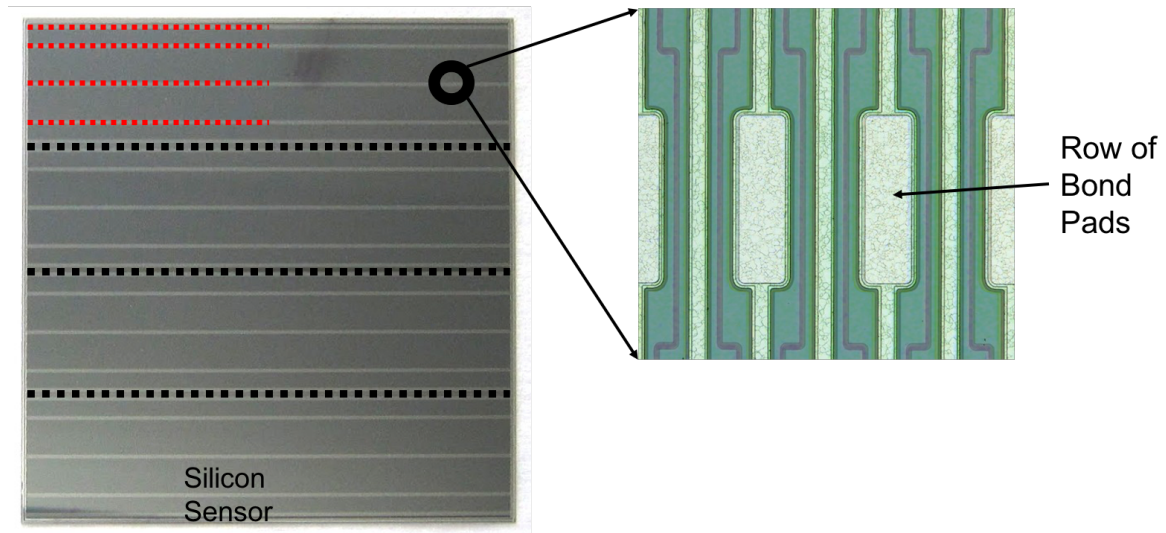


Figure 4: Illustration of a silicon sensor. Black dashed lines split it into 4 segments with 1024 sensor strips each. Every segment is split by red dashed lines, having 5 rows of wiring bond pad (as you can see in the right plot)

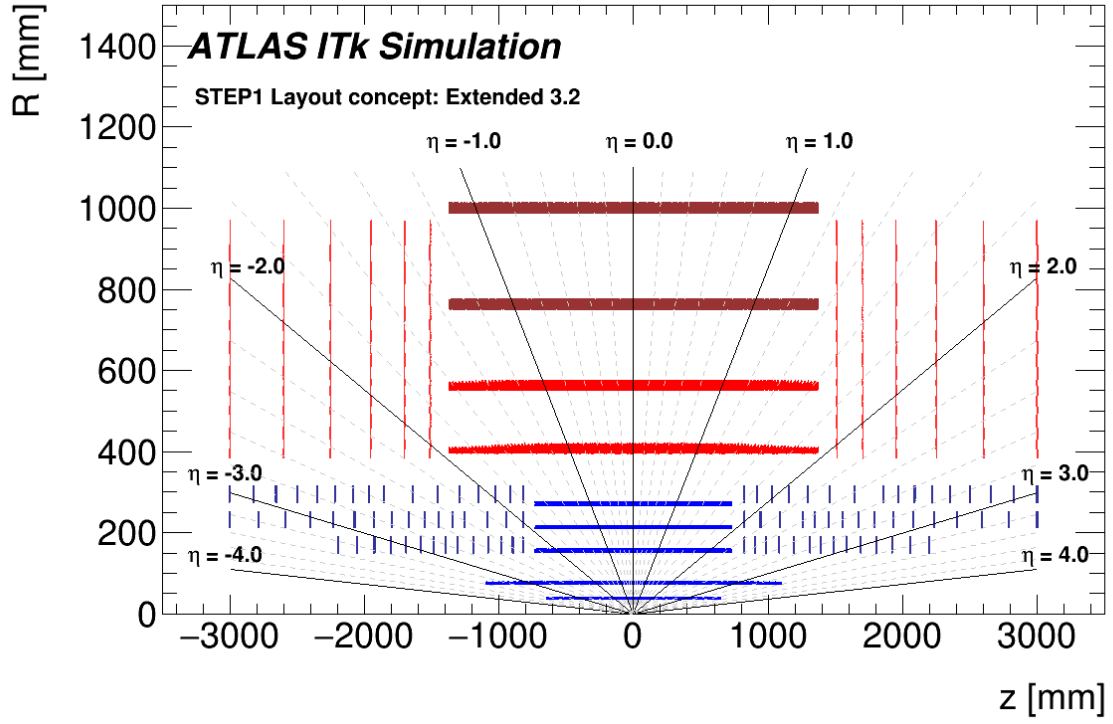


Figure 5: Extended_3.2 ITK layout in RZ direction. Blue lines represent the pixel detector; Red lines represent the strip detector (short strip: 23.8 mm); Brown lines represent the strip detector (long strip: 47.8mm);

measurement effects and helps the understanding of fake signals by statistically combined background signatures or falsely identified objects. In general, this requires a very detailed simulation of the physics process, and the way particles interact with the detector. Some mathematical problems arising from the theory of particles and their interaction with matter are simply impossible to solve analytically while others would take way to much time in doing so. Thus for particles passing through the ATLAS detector different MC methods are used to obtain the solutions.[7]

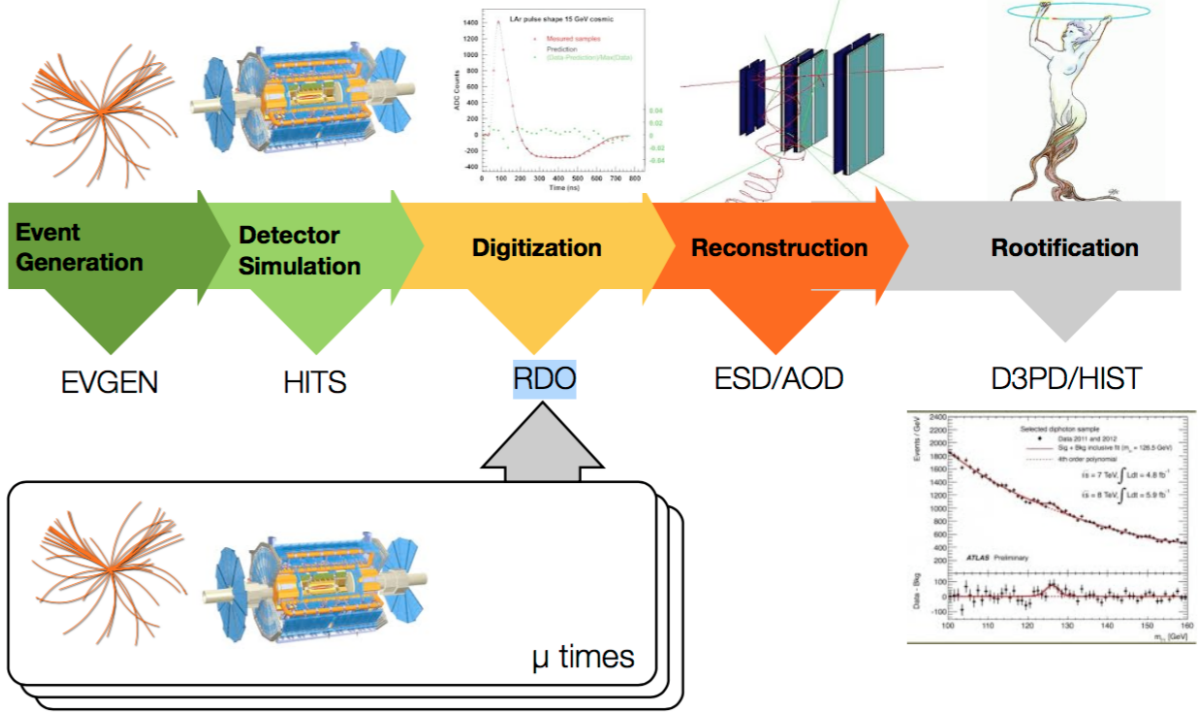


Figure 6: Illustration of the MC production chain for the MC11 and MC12 campaigns. The different output formats of the individual steps are shown. When emulating PU effects, pre-simulated HIT files are mixed given a chosen bunch structure schema with the simulated event at digitization stage.

See in figure 3. The first step in the MC production chain is the generation of the physics event by creating sets of 4-vectors. This step is in ATLAS typically carried out by event generators, such as PYTHIA and HERWIG. Decays of non-stable particles that do not reach the detector material are carried out by the event generator, stable or longer lived particles that are to decay in the detector volume are forwarded to the detector simulation. The output of the event generation are EVNT (EVGEN) files in the POOL/ROOT file format.

The next step is the simulation of the interaction of the particles with the sensitive and non-sensitive detector material. This can be achieved by a parametric smearing to model the detector response to a certain particle (likely to be used in a fast simulation), or a transport of the particle through the detector whereby each possible interaction is simulated in detail (as for the full simulation). The decay of non-stable particles not yet

carried out in the event generation is also performed and the decay products are further processed by the detector simulation. In sensitive detector elements, interacting particles create so called hits, which are collected for further processing in the digitization step. The output of the detector simulation is a HIT file in the POOL/ROOT file format. Hits created in the detector simulation need to be further processed to mimic the output of the detector readout. Common to all sub-detectors, however, is that the digitization deals with the noise modeling, channel masking and - most prominently in ATLAS - with the event pile-up. The output of the digitization step is a Raw Data Object (RDO) file in the POOL/ROOT file format, which is in the exact same format used to record real data.

Event reconstruction is performed on RDO files and consists of the local pattern recognition (i.e. the clustering and resolving of readout channels on the readout detector elements), reconstruction of tracks, segments, vertices, cells and clusters in the different sub-detectors, and finally the creation of high level objects, such as particles of different identification, jets including their flavor tag, or missing energy estimation. High level reconstruction objects are the input to the event analysis. The first output format of the reconstruction is the Event Summary Data (ESD), which is in a second step compressed to the so called Analysis Object Data (AOD) which is already the basis for many physics analysis. Both files are in the POOL/ROOT file format.

4 Experiment

Measurements[3] indicate that in bond pad rows, sensor strips with bond pads respond in areas where the the neighbor strip is expected to be (see in figure4). In order to estimate the impact on tracking under this circumstance, simulation on ITK tracking is needed.

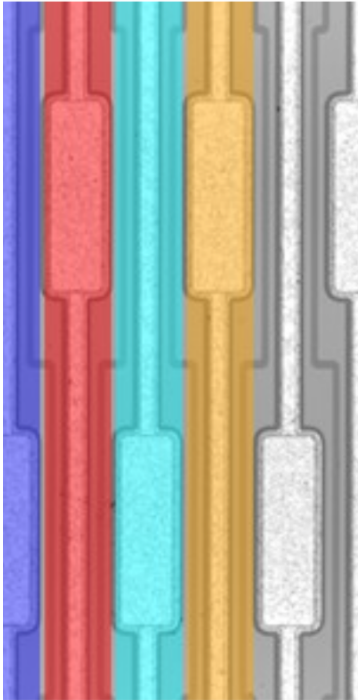
At first, choose the generated single muon samples with $p_T = 100$ GeV to make the simulation “clean”. The ITK layout would be Extended_3.2. When doing digitization, the “worst” scenario is considered, the activated strips happen to be wider on both sides of the sensor:

1. All the sensor strips on fire are randomly shifted in the neighbor one with shifting probability 7 %;
2. In the mean time, the two sides of the sensor strips should be correlated to be shifted in the same direction.

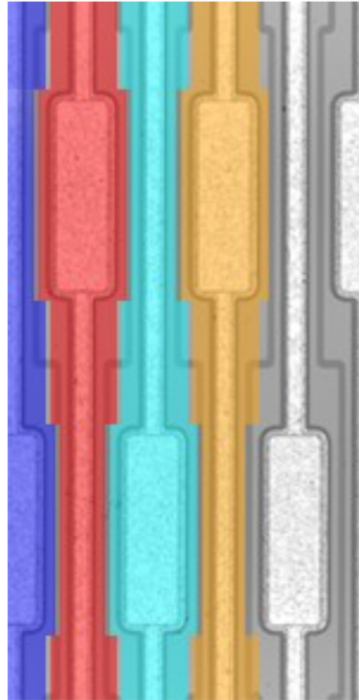
After reconstruction, two kinds of samples are gained. One is the nominal sample without any shifting, the other one is the shifted sample. As a comparison, the sample with two sides of sensor strips shifted in the opposite direction should be produced additionally (call it anti-shifted sample). In all three samples, truth tracks should pass truth track selections:

- The maximum absolute pseduorapidity should be 5 (the definition of pseduorapidity can be seen below);

Expected
responsive area:
 \pm strip pitch/2



Actual responsive
area: \pm strip pitch/2
+ bond pad area



Difference: strips
are wider around
bond pads

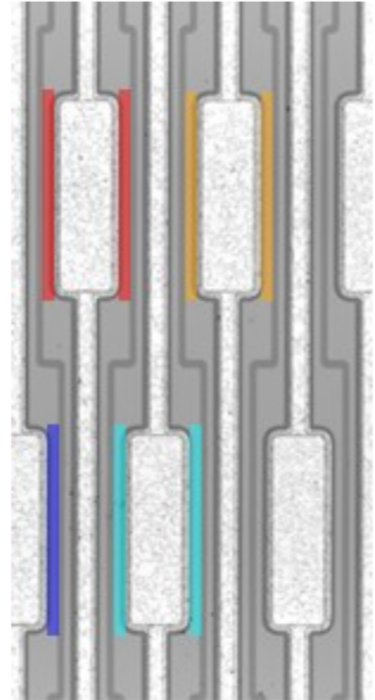


Figure 7: The difference between expected responding area and actual responding area in sensor bond pad regions. The left one is for expected, the area can correspond to strip pitch; The middle one is for actual, the area is wider/narrower for the channel with/without bond pads; The right one shows the difference, when a cluster hits in this region, the responding channel number is shifted by 1

- The minimum transverse momentum should be 900 MeV;
- The particle should be stable;
- The track should be charged;
- The particle should decay before arriving at pixel detectors (see in figure 1.1).

And reconstructed tracks should pass inner detector track selections:

- The minimum transverse momentum should be 900 MeV;
- The maximum transverse impact parameter should be 1 mm;
- The maximum longitudinal impact parameter should be 150 mm;
- The minimum number of silicon (pixel and SCT detectors) hits in a track should be 11;
- The maximum number of pixel holes¹ in a track should be 2;

There are 50000 entries in the single muon sample. After reconstruction, there are 50001 reconstructed tracks in the nominal sample, 49999 in the shifted sample; And after inner detector track selections, there are 47848\47793 selected tracks; At last, every selected track should match the truth track information stored in every event. There are eventually 47754\47645 matched tracks (see in table 4, 4). The less matched tracks in shifted sample shows that the impact of shifting strips is negative.

Table 1: The number of tracks in the nominal sample after every process and ratio among these processes including relative and total ratio.

Status	Number of tracks	Relative ratio	Total ratio
Reconstructed	50001	100.00%	100.00%
Selected	47848	95.69%	95.69%
Matched	47754	99.80%	95.51%

How to estimate the impact of shifting strips on ITK inner detector tracking? The track parameters should be first examined. A track in ATLAS is parametrized at the point of closest approach with the global Z-axis[1]:

d_0 The transverse impact parameter. The signed distance to the z-axis. See in figure 4.

z_0 The longitudinal impact parameter. The z-coordinate of the track at the point of closest approach to the global Z-axis.

¹The hole means after reconstruction there should be a hit on the detector along the track but isn't

Table 2: The number of tracks in the shifted sample after every process and ratio among these processes including relative and total ratio.

Status	Number of tracks	Relative ratio	Total ratio
Reconstructed	49999	100.00%	100.00%
Selected	47793	95.59%	95.59%
Matched	47645	99.69%	95.29%

ϕ_0 The angle with the x-axis in the X-Y plane at the perigee point.

θ The angle with the z-axis in the R-Z plane. The pseudorapidity $\eta = -\ln(\tan(\frac{\theta}{2}))$.

$\frac{q}{p}$ The charge of the particle divided by the momentum. $\frac{q}{p_T}$ and p_T are also used. p_T means transverse momentum.

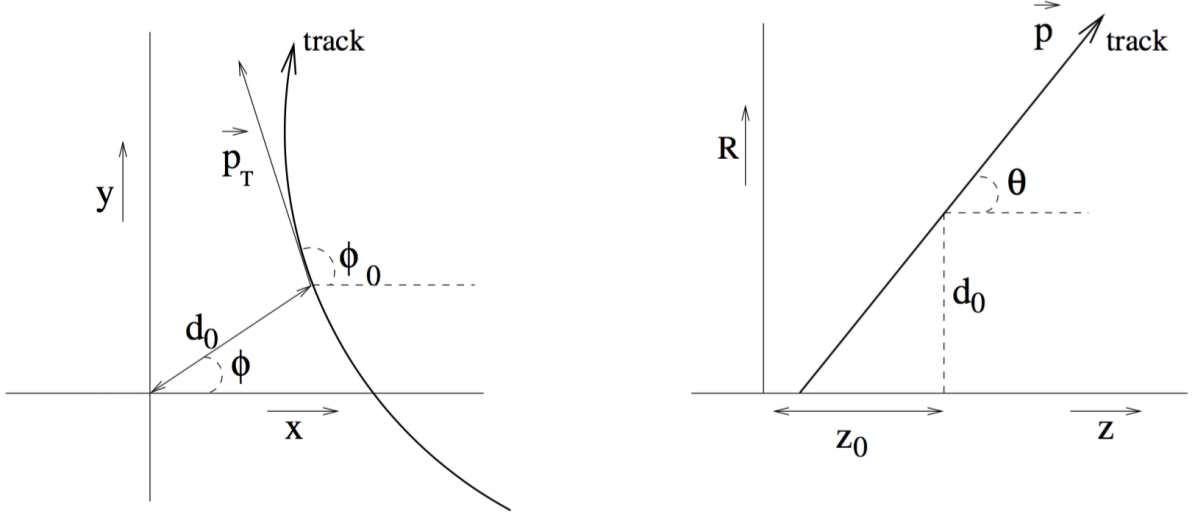


Figure 8: Illustration of the perigee parameters of a track in the transverse plane (left) and RZ-plane (right), as defined in the global ATLAS tracking frame

Figure 9 - 14 are selected track parameters' performance comparison between nominal and shifted samples. In each figure, the upper pad is the distribution as a function of track parameters. The Y-coordinate is the number of tracks within each bin. nominal and shifted samples are all drawn on it. The black line means nominal, while the blue line means shifted; The ratio of the number of tracks (shifted sample divided by nominal) is painted on the lower pad. Among these 5 track parameters, there is no remarkable difference on the performance of z_0 , η and ϕ parameters; And a measurable impact reflects on the performance of d_0 and p_T parameters.

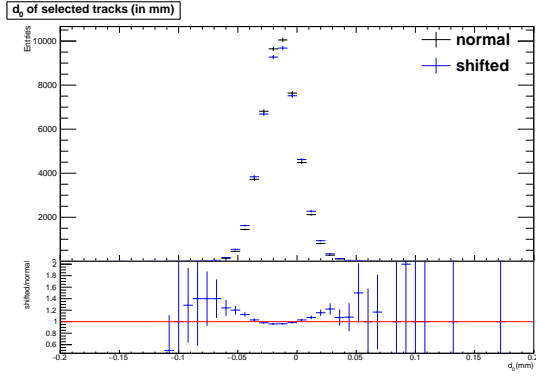


Figure 9: $d0$

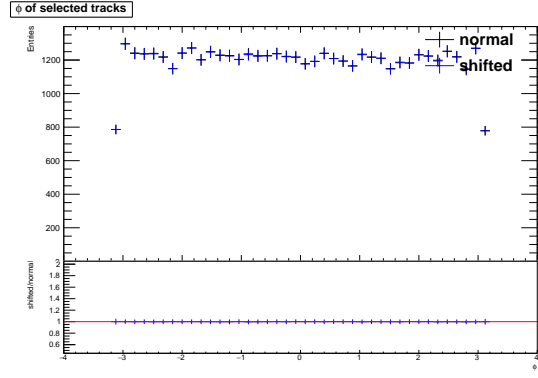


Figure 10: ϕ

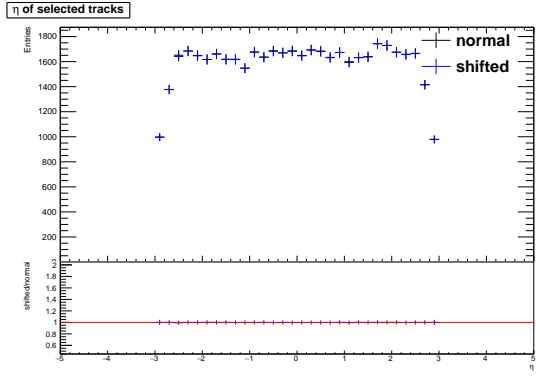


Figure 11: η

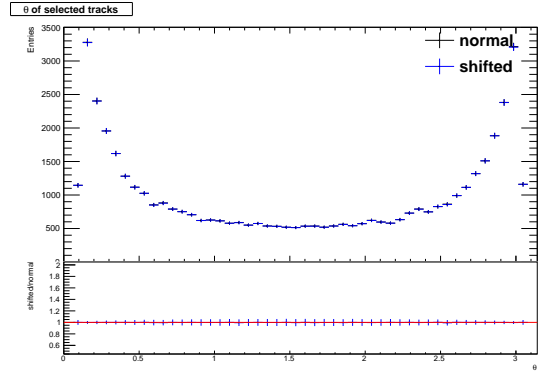


Figure 12: θ

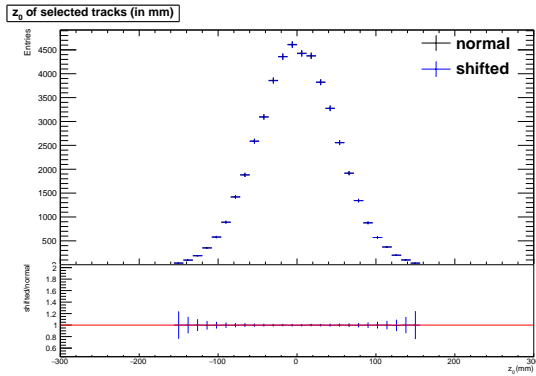


Figure 13: $z0$

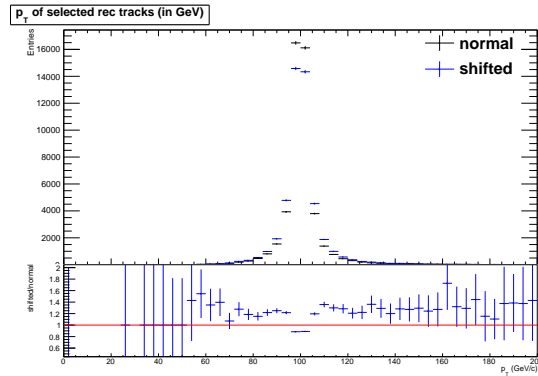
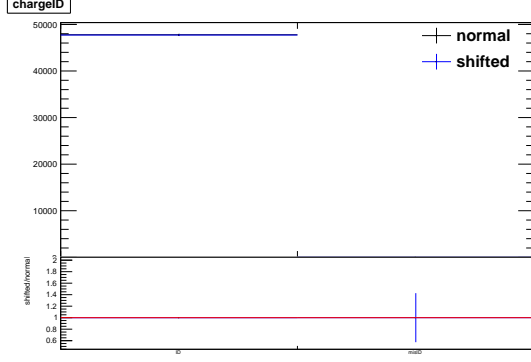
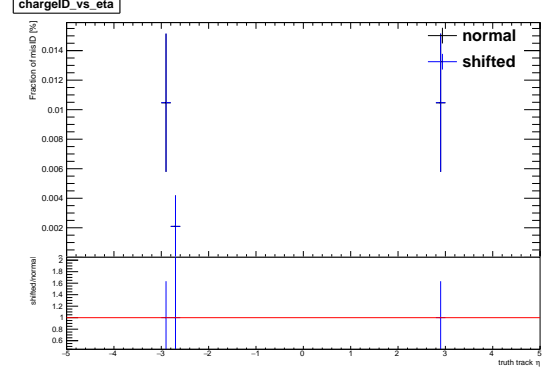


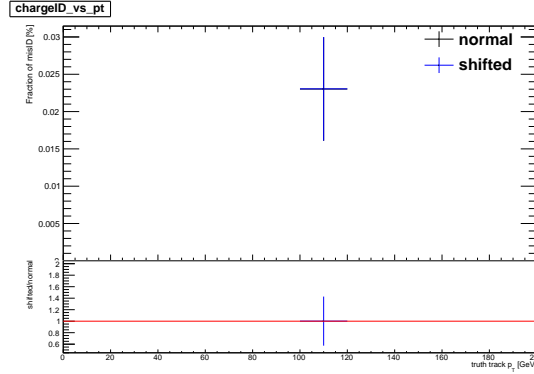
Figure 14: p_T



(a) Matched tracks' charge ID



(b) fraction versus η



(c) fraction versus p_T

Figure 15: (a) the number of matched tracks with and without correct chargeID. The number of mis-charged ID tracks of two samples is the same: 11; (b) The fraction of mis-charged ID tracks as a function of η ; (c) The fraction of mis-charged ID tracks as a function of p_T , which has a negligible difference

Figure 15(a) shows the number of matched tracks with and without correct chargeID. The first bin is the number of matched tracks with correct chargeID and the second shows tracks with mis-charged ID. Also dividing shifted sample by nominal sample to estimate the ratio. The fractions of mis-charged ID with two samples are almost the same and the value is so small: $\sim 0.02\%$, which is so good. Figure 15(b) - 15(c) shows the performance of η and p_T parameters of those mis-charged tracks. The independent variables are truth track η and p_T ; And the Y-coordinate shows the fraction of mis-charged ID (%). From these figures, the fractions are stable between nominal and shifted samples. It can be implied that this “worst” scenario has a negligible impact on the resolution of charge. Among track parameters mentioned above, a remarkable impact can be seen on the performances of transverse variables like d_0 and p_T . A further study should investigate how these 2 parameters vary as functions of other variables like η and ϕ to try to figure out the details about this influence. Then the efficiency of reconstructed tracks matching the

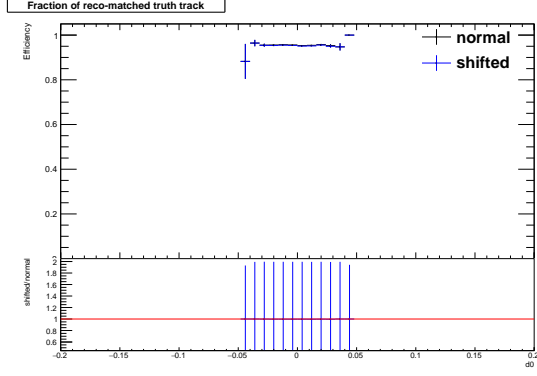
truth should be considered. Figure 16 show the efficiency varies as a function of track parameters. Here choose matched truth tracks' information to fill histograms. Also in the upper pad, black line means nominal sample's efficiency while blue line means shifted sample's. And in the lower pad, a ratio is gotten by dividing shifted sample's efficiency by nominal sample's. Among these 5 figures, all efficiency is very similar with each other. Although It looks like the matched truth track efficiency is a bit different as a function of ϕ , the ratio is quite close to 1. Most efficiency of each bin are less than 1, means the the impact of shifting strips' hit positions is negative.

As mentioned above, $d0$ and p_T distributions as functions of other parameters should be investigated, of which the comparison of two samples about $d0$ resolution as functions of η and p_T somehow in replace temporarily has been analysed because of the limited time. Figures 17 and 18 show track parameters' resolutions as functions of η and p_T . The resolution means $V_{reco} - V_{truth}$ of track parameters within reconstructed matched tracks. There should be 2D plots performing parameters' resolution as functions of η and p_T (see in figure 19 showing $d0$ resolution as functions of η and p_T as an example). For comparing differences with two samples easily, taking $d0$ resolution as a function of η for instance, get the mean value and the error of $d0$ resolution in every η bin. Therefore 2 plots are produced standing for the 2D resolution plot.

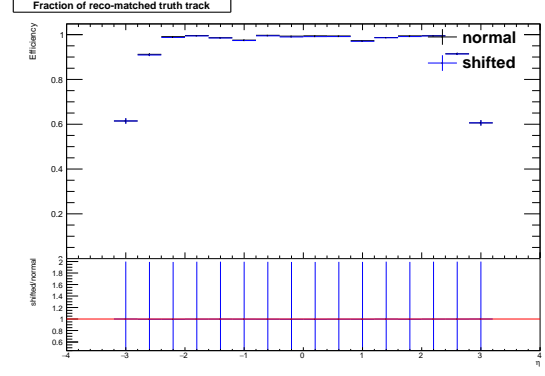
In figures 17 and 18, the left column stays resolutions' mean value versus η and p_T , the right stays the error of it. As usual the black line stands for the nominal sample distribution and the blue line stands for the shifted sample. Among these parameters' resolutions, although all have sizable differences between two samples, only the ratios of $d0$, ϕ and $\frac{d}{p_T}$ resolutions' mean values indeed differ with 1. For other parameters, 1 is just in error regions, which can be explained implicitly the shifting has a remarkable effect on transverse parameters. And there is one more statement most errors of the mean values of parameters' resolutions in shifted sample are larger than those in nominal sample. Also events' transverse momentum distribution is so narrow that a judgment can't be made arbitrarily.

5 Conclusion

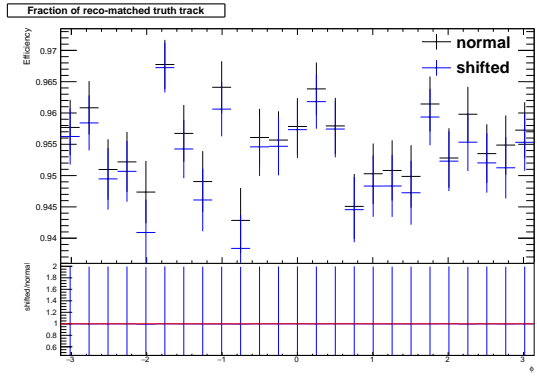
Because strips with bond pads are wider than the neighbor one, they respond in areas where the neighbor strip is expected to be, which may have effects on track reconstruction. In order to evaluate this influence, a "worst" scenario was proposed. Single muon samples with 50000 events was chosen. Found that such shifts indeed have a measurable effect on the reconstructed track parameters, especially on $d0$, ϕ and p_T distribution. Next studies should focus on how this effect varies as a function of p_T and particle types to find true effects on the detector reconstruction. Then some optimizations may be selected to minimize this effect.



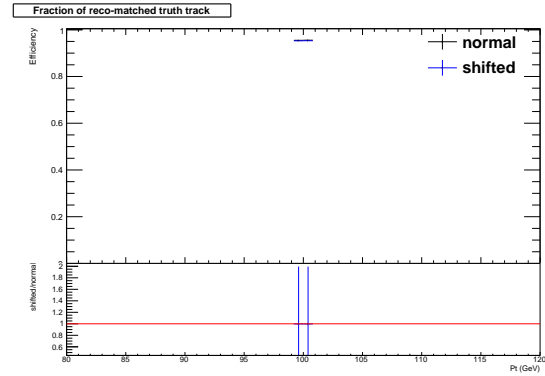
(a) d_0



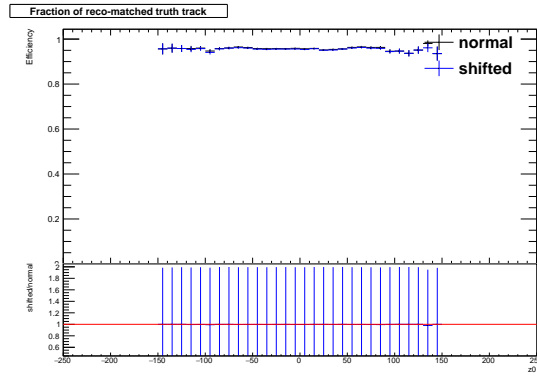
(b) η



(c) ϕ

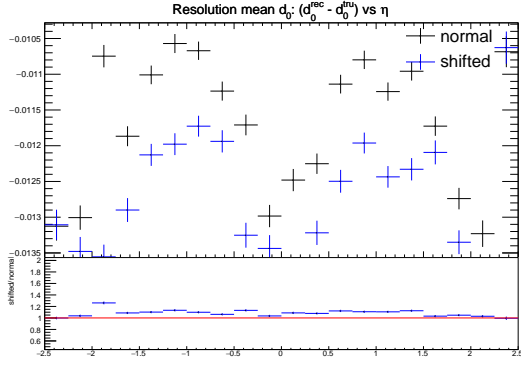


(d) p_T

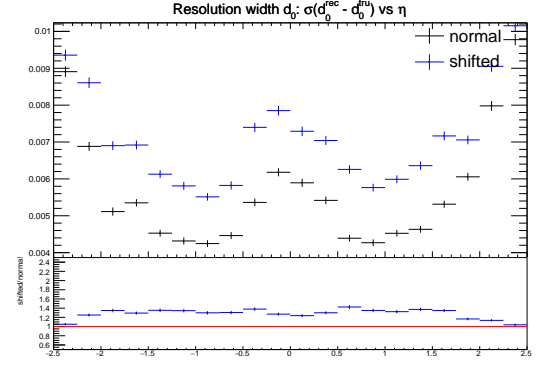


(e) z_0

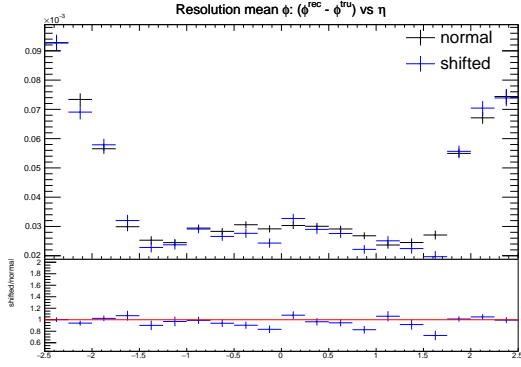
Figure 16: (a) The efficiency as a function of d_0 ; (b) The efficiency as a function of η ; (c) The efficiency as a function of ϕ , the ratio is very close to 1 although differences can be seen from the comparison of shifted sample between nominal sample; (d) The efficiency as a function of p_T ; (e) The efficiency as a function of z_0



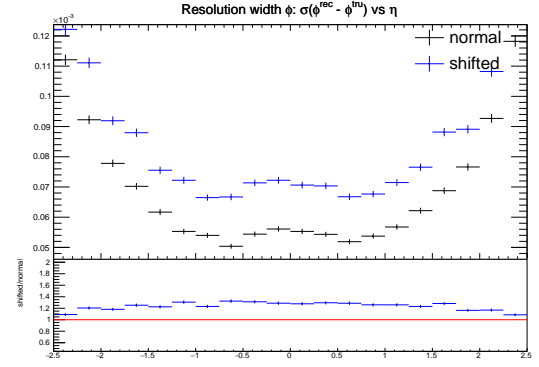
(a) Mean: $d0$ vs η



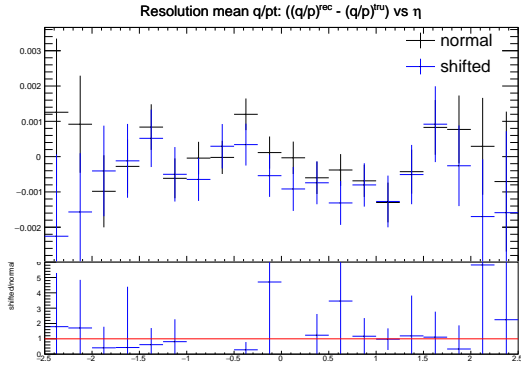
(b) Width: $d0$ vs η



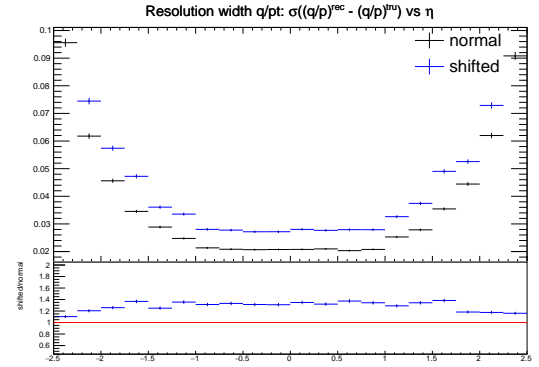
(c) Mean: ϕ vs η



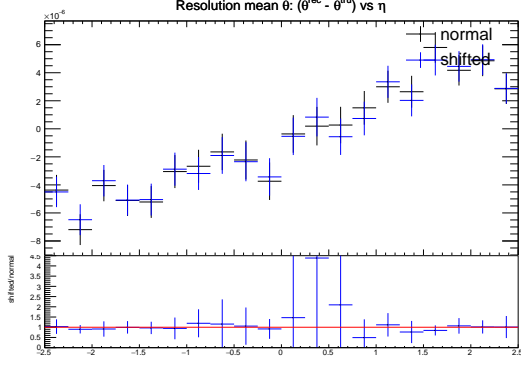
(d) Width: ϕ vs η



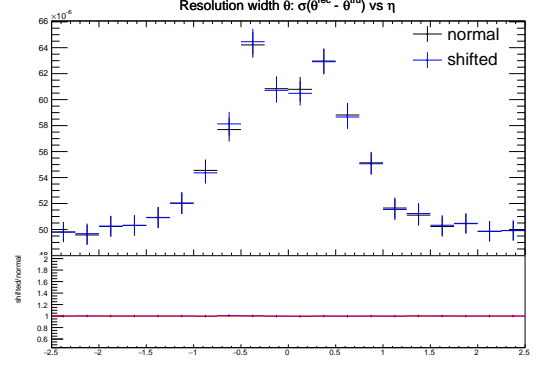
(e) Mean: $\frac{q}{p_T}$ vs η



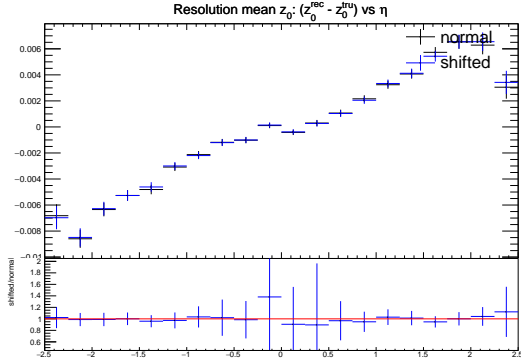
(f) Width: $\frac{q}{p_T}$ vs η



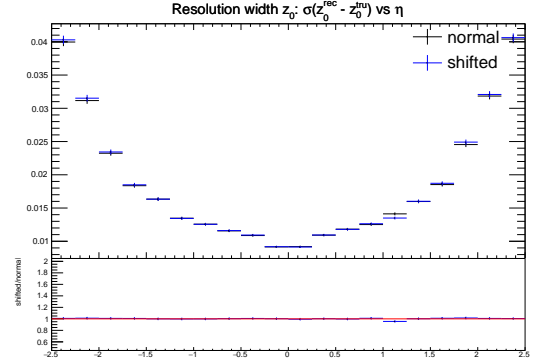
(g) Mean: θ vs η



(h) Width: θ vs η

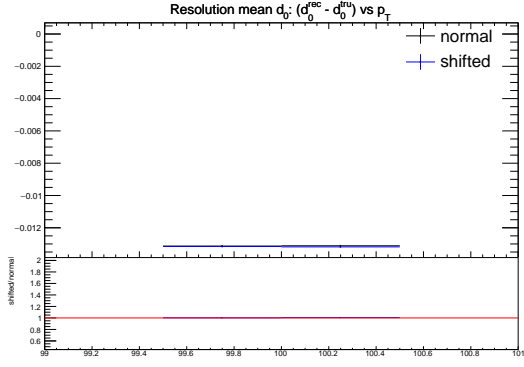


(i) Mean: z_0 vs η

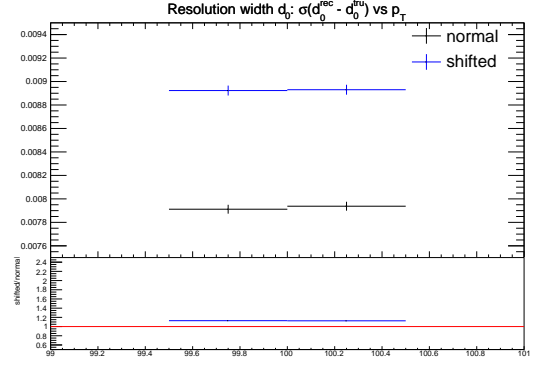


(j) Width: z_0 vs η

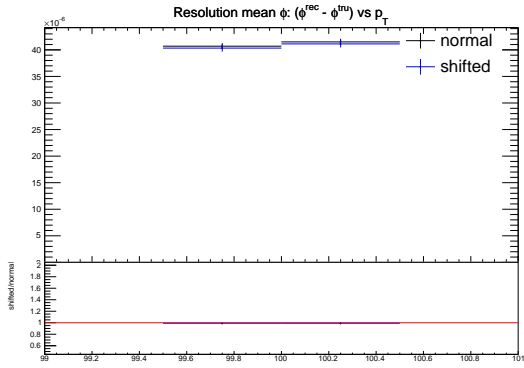
Figure 17: (a) The mean value of d_0 resolution versus η ; (b) The error of mean value of d_0 resolution versus η ; (c) The mean value of ϕ resolution versus η ; (d) The error of mean value of ϕ resolution versus η ; (e) The mean value of $\frac{q}{p_T}$ resolution versus η ; (f) The error of mean value of $\frac{q}{p_T}$ resolution versus η ; (g) The mean value of θ resolution versus η ; (h) The error of mean value of θ resolution versus η ; (i) The mean value of z_0 resolution versus η ; (j) The error of mean value of z_0 resolution versus η



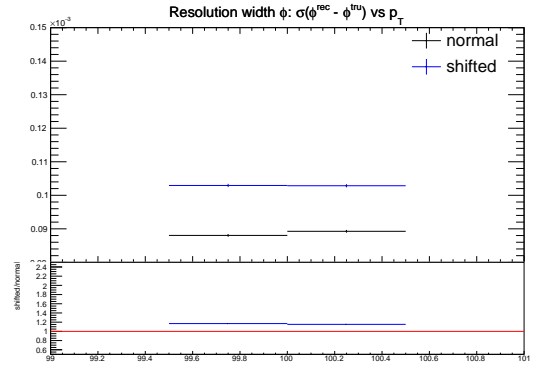
(a) Mean: d_0 vs p_T



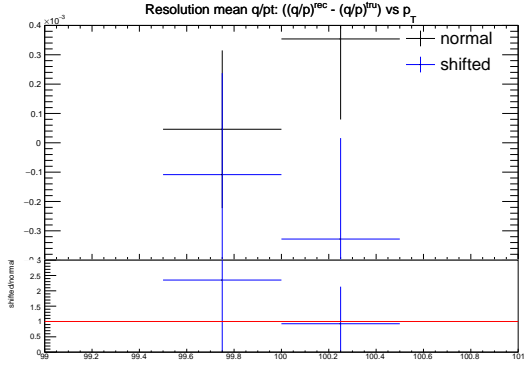
(b) Width: d_0 vs p_T



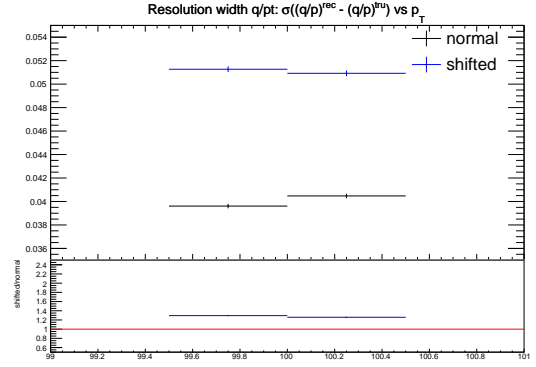
(c) Mean: ϕ vs p_T



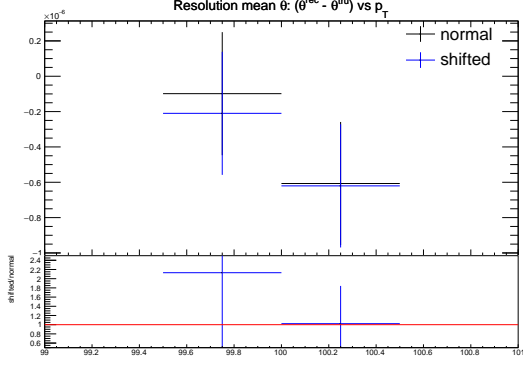
(d) Width: ϕ vs p_T



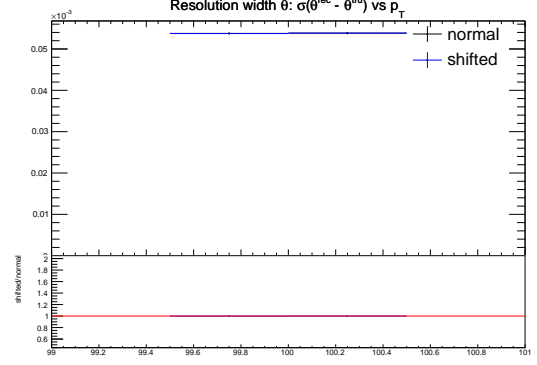
(e) Mean: $\frac{q}{p_T}$ vs p_T



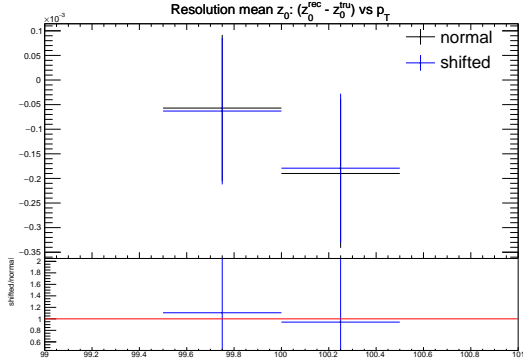
(f) Width: $\frac{q}{p_T}$ vs p_T



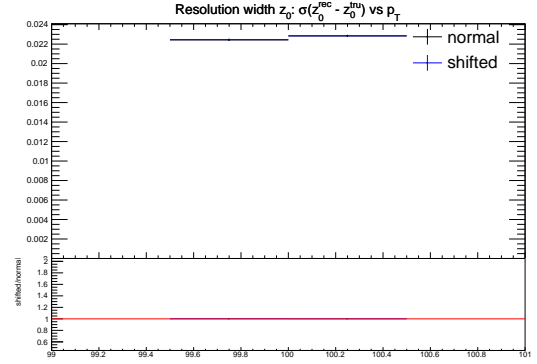
(g) Mean: θ vs p_T



(h) Width: θ vs p_T



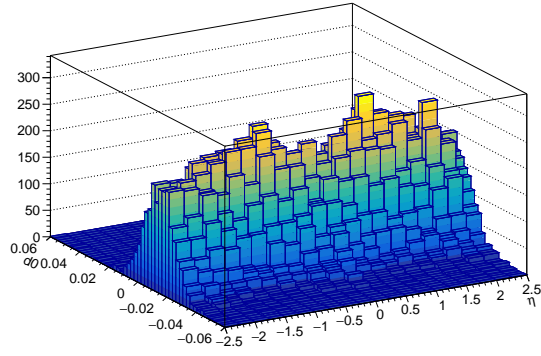
(i) Mean: z_0 vs p_T



(j) Width: z_0 vs p_T

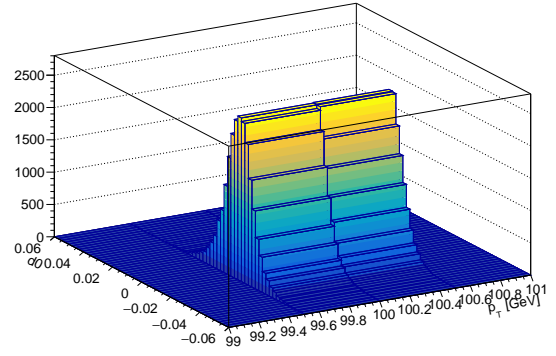
Figure 18: (a) The mean value of $d0$ resolution versus p_T ; (b) The error of mean value of $d0$ resolution versus p_T ; (c) The mean value of ϕ resolution versus p_T ; (d) The error of mean value of ϕ resolution versus p_T ; (e) The mean value of $\frac{q}{p_T}$ resolution versus p_T ; (f) The error of mean value of $\frac{q}{p_T}$ resolution versus p_T ; (g) The mean value of θ resolution versus p_T ; (h) The error of mean value of θ resolution versus p_T ; (i) The mean value of $z0$ resolution versus p_T ; (j) The error of mean value of $z0$ resolution versus p_T

Resolution d_0 : $(d_0^{\text{rec}} - d_0^{\text{tru}})$ vs η



(a) Resolution: $d0$ vs η

Resolution d_0 : $(d_0^{\text{rec}} - d_0^{\text{tru}})$ vs p_T



(b) Resolution: $d0$ vs p_T

Figure 19: (a) $d0$ resolution as a function of η ; (b) $d0$ resolution as a function of p_T

References

- [1] Track and vertex reconstruction in the ATLAS inner detector *Maaïke Limper*
- [2] The ATLAS ITk Strip Detector. Status of R&D *Carlos García Argos, on behalf of the ATLAS ITk Strip Collaboration*
- [3] Silicon strip sensor architecture concessions to module building requirements and their impact on tracking performance *Luise Poley, on behalf of the ATLAS Collaboration*
- [4] The ATLAS upgrade program *Claudia Gemme, On behalf of the ATLAS Collaboration, Istituto Nazionale di Fisica Nucleare, Genova, Italy*
- [5] About the ATLAS Experiment <https://atlas.cern/discover/about>
- [6] The Detector <https://atlas.cern/discover/detector>
- [7] TRUTH SEEDED RECONSTRUCTION FOR FAST SIMULATION IN THE ATLAS EXPERIMENT *Roland Jansky*
- [8] Initial Design Report for the ITk *ATLAS Collaboration*